Domain decomposition and upscaling technique for metascreens

Michael Leumüller, Karl Hollaus and Joachim Schöberl
Institute for Analysis and Scientific Computing, Technische Universität Wien, Vienna, Austria

Received 8 March 2021
Revised 28 September 2021
25 November 2021
Accepted 14 February 2022

Abstract

Purpose – This paper aims to consider a multiscale electromagnetic wave problem for a housing with a ventilation grill. Using the standard finite element method to discretise the apertures leads to an unduly large number of unknowns. An efficient approach to simulate the multiple scales is introduced. The aim is to significantly reduce the computational costs.

Design/methodology/approach – A domain decomposition technique with upscaling is applied to cope with the different scales. The idea is to split the domain of computation into an exterior domain and multiple non-overlapping sub-domains. Each sub-domain represents a single aperture and uses the same finite element mesh. The identical mesh of the sub-domains is efficiently exploited by the hybrid discontinuous Galerkin method and a Schur complement which facilitates the transition from fine meshes in the sub-domains to a coarse mesh in the exterior domain. A coarse skeleton grid is used on the interface between the exterior domain and the individual sub-domains to avoid large dense blocks in the finite element discretisation matrix.

Findings – Applying a Schur complement to the identical discretisation of the sub-domains leads to a method that scales very well with respect to the number of apertures.

Originality/value – The error compared to the standard finite element method is negligible and the computational costs are significantly reduced.

Keywords Finite element method, Domain decomposition method, Metasurfaces

Paper type Research paper

1. Introduction

In the context of electromagnetic compatibility, ventilation grills are also called metascreens (Holloway and Kuester, 2018). Such geometries contain regions with a locally periodic structure, for example, openings or scattering objects. This property will be called quasi-periodic. Around these objects a fine mesh is needed in finite element (FE) simulations. The goal of this work is to improve the computational times in electromagnetic wave simulations by reducing the degrees of freedom.

Many different methods have been considered in simulating shieldings with apertures. In the time domain setting, the finite difference time domain method (FDTD) is prominent and has been considered, for example, in Georgakopoulos *et al.* (2001) and Jiao *et al.* (2006). For simulations in the frequency domain, the method of moments (MoM) (Araneo and Lovat, 2009), the finite element

The authors acknowledge support from the Austrian Science Fund (FWF) through grant number W1245 and the support by the "University SAL Labs" initiative of Silicon Austria Labs (SAL) and its Austrian partner universities for applied fundamental research for electronic-based systems.

COMPEL - The international journal for computation and mathematics in electrical and electronic engineering
Vol. 41 No. 3, 2022
pp. 938-953
Emerald Publishing Limited
0332-1649
DOI 10.1108/COMPEL-03-2021-0073

method (FEM) (Kubík and Skála, 2015; Carpes *et al.*, 2000; Boubekeur *et al.*, 2014) or transmission line models (TLM) (Carpes *et al.*, 2000; Nie *et al.*, 2011) are common. The cited works above mainly focus on shieldings with a single or few apertures. The present work deals with simulations for shieldings with many apertures. In Ali *et al.* (2005) and Li *et al.* (2000) the FDTD and the MoM are considered for such examples. Another approach for large numbers of quasi-periodic apertures is homogenisation which has been studied in Bardi *et al.* (2006) and Cruciani *et al.* (2015). In this work, the idea of the Nitsche-type mortaring finite element method for the vector potential wave equation considering non-matching meshes introduced in Hollaus *et al.* (2010) and Heinrich and Nicaise (2001) is altered to fit the quasi-periodic setting with many apertures.

The method will be used to establish an upscaling by non-matching meshes. In (Heinrich and Nicaise, 2001) the structure of the resulting system matrix is exploited to reduce the computational effort of solving the system of linear equations by applying a Schur Complement (SC). This work applies the method to the electromagnetic wave problem with multiple sub-domains. The main contribution of this work is the efficient implementation of a SC for quasi-periodic structures. This is achieved by discretising each aperture identically.

The weak formulation for the vector potential wave equation in the time harmonic setting is derived in Section 2. The quasi-periodic structure is exploited via a domain decomposition (DD) approach where many of the generated sub-domains are identical. This property is further used by introducing non-matching meshes, leading to an upscaling (Graham and Scheichl, 2007) and applying the Nitsche-type mortar finite element method (NMFEM) (Hollaus *et al.*, 2010) to cope with the non-matching mesh in Section 3. In Section 4 the resulting system matrix for the NMFEM and its special structure are highlighted. To exploit this structure a SC is applied, to effectively eliminate all the sub-domains from the computation reducing the computation time, in Section 5. The proposed method is applied to various electromagnetic wave problems for 2 D geometries as well as 3 D geometries, in Section 6. The computational times for the NMFEM and the FEM are compared in Section 6.

2. Domain decomposition with upscaling for the time harmonic wave equation

The vector potential wave equation in the time harmonic setting using a magnetic vector potential $\mathbf{A}$ is given as:

$$\operatorname{curl}\mu^{-1}\operatorname{curl}\mathbf{A} - \kappa^2\mathbf{A} = 0 \text{ in } \Omega, \tag{1}$$

$$\mathbf{A}\times\mathbf{n} = 0 \text{ on } \Gamma_D, \tag{2}$$

$$\mu^{-1}\operatorname{curl}\mathbf{A}\times\mathbf{n} = 0 \text{ on } \Gamma_N, \tag{3}$$

$$\mu^{-1}\operatorname{curl}\mathbf{A}\times\mathbf{n} + \frac{j\omega}{Z}(\mathbf{n}\times\mathbf{A})\times\mathbf{n} = 0 \text{ on } \Gamma_t, \tag{4}$$

$$\mu^{-1}\operatorname{curl}\mathbf{A}\times\mathbf{n} + \frac{j\omega}{Z}(\mathbf{n}\times\mathbf{A})\times\mathbf{n} = \mathbf{h}\times\mathbf{n} \text{ on } \Gamma_e \tag{5}$$

with $\kappa^2 = j\omega\sigma + \omega^2\varepsilon$ and $\Omega = \bigcup_{i=0}^{n}\Omega_i \subset \mathbb{R}^3$. The physical parameters μ, ε and σ are the magnetic permeability, the electric permittivity and the conductivity, respectively, $\omega = 2\pi f$ is the angular frequency, j is the imaginary unit, $\mathbf{h}$ is a prescribed boundary field and

$Z = \sqrt{\frac{\mu}{\varepsilon}}$ is the wave impedance. Sub-domains are defined in Figure 1. To derive the, for FEM needed, weak formulation the following function spaces are needed:

$$L^2(\Omega) := \{\mathbf{v} : \Omega \to \mathbb{C}; \int_\Omega |\mathbf{v}|^2 \, d\mathbf{x} < \infty\}, \tag{6}$$

$$H(\mathrm{curl}, \Omega) := \{\mathbf{v} \in \left[L^2(\Omega)\right]^3; \mathrm{curl}\mathbf{v} \in \left[L^2(\Omega)\right]^3\}, \tag{7}$$

$$H_0(\mathrm{curl}, \Omega) := \{\mathbf{v} \in H(\mathrm{curl}, \Omega); \mathbf{v} \times \mathbf{n}|_{\Gamma_D} = 0\}, \tag{8}$$

$$L^2(\Gamma) := \{\mathbf{v} : \Gamma \to \mathbb{C}; \int_\Gamma |\mathbf{v}|^2 \, d\mathbf{s} < \infty\}. \tag{9}$$

Equation (1) is multiplied by $\mathbf{v} \in H_0(\mathrm{curl}, \Omega)$ and then integration by parts is carried out. This leads to the weak formulation: Find $\mathbf{A} \in H_0(\mathrm{curl}, \Omega)$ so that:

$$\int_\Omega \mu^{-1} \mathrm{curl}\, \mathbf{A} \cdot \mathrm{curl}\mathbf{v} - \kappa^2 \mathbf{A} \cdot \mathbf{v} \, d\mathbf{x} - \frac{j\omega}{Z} \int_{\Gamma_e \cup \Gamma_t} \mathbf{A} \times \mathbf{n} \cdot \mathbf{v} \times \mathbf{n} \, d\mathbf{s} = \int_{\Gamma_e} \mathbf{h} \times \mathbf{n} \cdot \mathbf{v} \times \mathbf{n} \, d\mathbf{s} \tag{10}$$

for all $\mathbf{v} \in H_0(\mathrm{curl}, \Omega)$.

To be able to exploit the quasi-periodic structure the whole domain is decomposed into the exterior domain Ω_0 and the sub-domains $\Omega_i, i \in \{1, \ldots, n\}$, see Figure 1. The domains are non-overlapping and share the interface Γ. This interface is not only between Ω_0 and the Ω_i, but also between the sub-domains. The Ω_i are chosen such that each represents exactly one aperture and Ω_0 encloses all Ω_i. In the decomposition the sub-domains are geometrically identical; therefore, each can be discretised in the same way. This means that, independent of the number of apertures, only one Ω_i has to be meshed and the FE system matrix for just a single sub-domain needs to be assembled.

The DD can be used to address a second issue. The small geometric structure around an aperture leads to a very fine discretisation. This entails a fine discretisation in the vicinity of

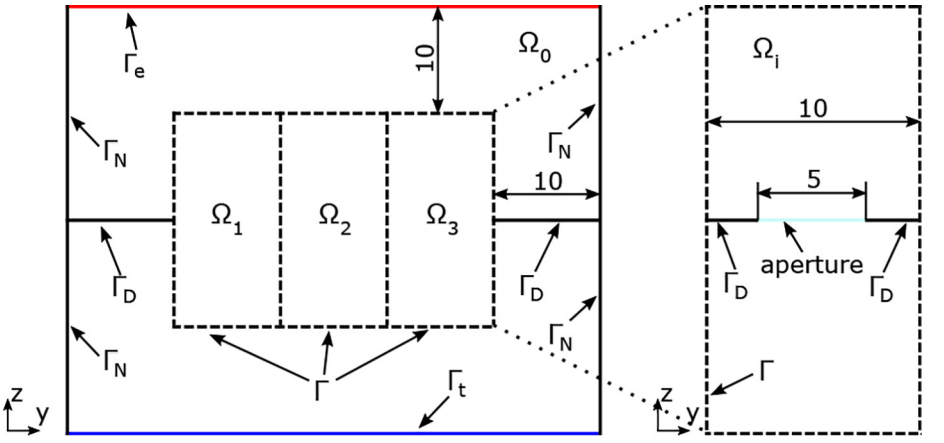

Figure 1.
Domain decomposition of the domain (left) into the exterior domain Ω_0 and the sub-domains Ω_i (right)

Note: The interface Γ is indicated by dashed lines, all dimensions are in mm

the aperture due to the necessarily regular, conforming mesh for the FEM. A sufficiently accurate solution could be represented by a coarser mesh; therefore, the fine mesh unnecessarily increases the computational costs. The goal is to discretise the exterior domain as coarse as possible such that the wave propagation is appropriately resolved and at the same time discretise the sub-domains fine enough to grasp the local, small-scale behaviour of the solution around the apertures. This leads to an upscaling between the solutions on the Ω_i and the solution on Ω_0. The resulting non-conforming mesh over Γ can be seen in Figure 2 and 3. The FEM is not capable to cope with non-conforming meshes. To address this issue the NMFEM is applied.

3. Nitsche-type mortar finite element method

The general idea of the NMFEM is to break the strong continuity of the FE solution on domain boundaries and reinforce it in a weak sense. This is achieved by introducing a FE space $X(\Gamma) = \left[L^2(\Gamma)\right]^3$ which is defined on Γ, see Figure 3. Using the NMFEM, the FEs on different sub-domains are not coupled directly, but only via the interface FEs on Γ. In an usual discontinuous Galerkin method the continuity of the numerical flux is enforced by testing with test functions from both side of the interface, which leads to a coupling between elements. This is avoided by the NMFEM, because the continuity of the normal flux across interfaces is tested by new interface variables. Therefore FEs on different sub-domains do not couple directly (Hollaus *et al.*, 2010; Cockburn *et al.*, 2009).

3.1 NMFEM for the time harmonic wave equation

The vector potential wave equation in the time harmonic setting using local magnetic vector potentials $\mathbf{A}_i$ for each sub-domain is given as:

$$\mathrm{curl}\,\mu^{-1}\mathrm{curl}\mathbf{A}_i - \kappa^2\mathbf{A}_i = 0 \text{ in } \Omega_i, \tag{11}$$

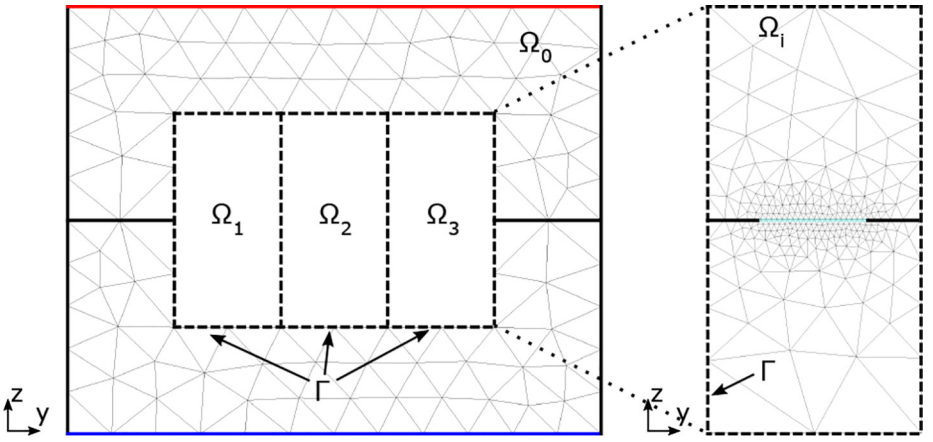

Note: The interface Γ is indicated by dashed lines

Figure 2. Coarse mesh on the exterior domain (left), fine mesh on the sub-domain (right)

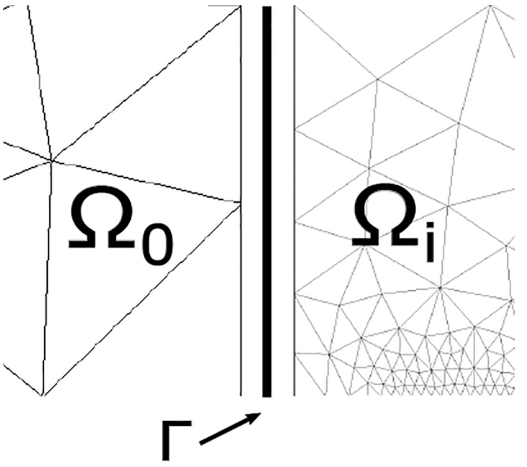

Figure 3.
A detail of the interface Γ between Ω_0 and Ω_i on which the interface finite element space is defined

$$\mathbf{A}_i \times \mathbf{n}_i = -\mathbf{A}_j \times \mathbf{n}_j =: \hat{\mathbf{A}} \times \mathbf{n}_i \text{ on } \Gamma, \tag{12}$$

$$\mu^{-1}\text{curl}\mathbf{A}_i \times \mathbf{n}_i + \mu^{-1}\text{curl}\mathbf{A}_j \times \mathbf{n}_j = 0 \text{ on } \Gamma, \tag{13}$$

$$\mathbf{A}_i \times \mathbf{n}_i = 0 \text{ on } \Gamma_D, \tag{14}$$

$$\mu^{-1}\text{curl}\mathbf{A}_0 \times \mathbf{n}_0 = 0 \text{ on } \Gamma_N, \tag{15}$$

$$\mu^{-1}\text{curl}\mathbf{A}_0 \times \mathbf{n}_0 + \frac{j\omega}{Z}(\mathbf{n}_0 \times \mathbf{A}_0) \times \mathbf{n}_0 = 0 \text{ on } \Gamma_t, \tag{16}$$

$$\mu^{-1}\text{curl}\mathbf{A}_0 \times \mathbf{n}_0 + \frac{j\omega}{Z}(\mathbf{n}_0 \times \mathbf{A}_0) \times \mathbf{n}_0 = \mathbf{h} \times \mathbf{n}_0 \text{ on } \Gamma_e. \tag{17}$$

The vector $\mathbf{n}_i$ is the outward pointing normal vector on the boundary of Ω_i. The tangential continuity of the $\mathbf{A}_i$ over Γ is enforced by equation (12). The vector field $\hat{\mathbf{A}}$ represents the tangential component of the $\mathbf{A}_i$ and is needed to derive the weak formulation for the NMFEM. The tangential continuity of the flux is ensured by equation (13).

To obtain the weak formulation for the NMFEM, equation (11) is multiplied with a test function $\mathbf{v}_i \in H_0(\text{curl}, \Omega_i)$ on each domain and then integration by parts is carried out. This leads to the initial weak formulation:

$$\sum_i \int_{\Omega_i} \mu^{-1}\mathrm{curl}\mathbf{A}_i \cdot \mathrm{curl}\mathbf{v}_i - \kappa^2 \mathbf{A}_i \cdot \mathbf{v}_i \, d\mathbf{x} - \int_{\Gamma} \left(\mu^{-1}\mathrm{curl}\mathbf{A}_i \times \mathbf{n}_i\right) \cdot \mathbf{v}_i \, d\mathbf{s}$$

$$-\frac{j\omega}{Z} \int_{\Gamma_e \cup \Gamma_t} \mathbf{A}_0 \times \mathbf{n}_0 \cdot \mathbf{v}_0 \times \mathbf{n}_0 \, d\mathbf{s} = \int_{\Gamma_e} \mathbf{h} \times \mathbf{n}_0 \cdot \mathbf{v}_0 \times \mathbf{n}_0 \, d\mathbf{s}. \tag{18}$$

This closely resembles equation (10) with the difference that the volume term is separated into the sub-domains and due to the fact that the solution is not continuous over Γ, the boundary integrals appear. This weak formulation is incomplete in the sense that the continuity over Γ is not yet considered. To be able to enforce the field trace continuity in equation (12) and equation (13), a vector valued space $X(\Gamma)$ of traces of Nédélec kind [Schöberl and Zaglmayr (2005)] are needed. Multiplying equation (13) with $\hat{\mathbf{v}} \in X(\Gamma)$ and integrating over Γ leads to the term:

$$0 = \int_{\Gamma} \left(\mu^{-1}\mathrm{curl}\mathbf{A}_i \times \mathbf{n}_i + \mu^{-1}\mathrm{curl}\mathbf{A}_j \times \mathbf{n}_j\right) \cdot \hat{\mathbf{v}} \, d\mathbf{s}, \tag{19}$$

which is zero if the flux of the solution is continuous. Adding this term to equation (18) yield:

$$\sum_i \int_{\Omega_i} \mu^{-1}\mathrm{curl}\mathbf{A}_i \cdot \mathrm{curl}\mathbf{v}_i - \kappa^2 \mathbf{A}_i \cdot \mathbf{v}_i \, d\mathbf{x} - \int_{\Gamma} \left(\mu^{-1}\mathrm{curl}\mathbf{A}_i \times \mathbf{n}_i\right) \cdot (\mathbf{v}_i - \hat{\mathbf{v}}) \, d\mathbf{s}$$

$$-\frac{j\omega}{Z} \int_{\Gamma_e \cup \Gamma_t} \mathbf{A}_0 \times \mathbf{n}_0 \cdot \mathbf{v}_0 \times \mathbf{n}_0 \, d\mathbf{s} = \int_{\Gamma_e} \mathbf{h} \times \mathbf{n}_0 \cdot \mathbf{v}_0 \times \mathbf{n}_0 \, d\mathbf{s}. \tag{20}$$

Using:

$$\left(\mu^{-1}\mathrm{curl}\mathbf{A}_i \times \mathbf{n}_i\right) \cdot (\mathbf{v}_i - \hat{\mathbf{v}}) = -\mu^{-1}\mathrm{curl}\mathbf{A}_i \cdot (\mathbf{v}_i - \hat{\mathbf{v}}) \times \mathbf{n} \tag{21}$$

for the boundary term and adding:

$$\sum_i \int_{\Gamma} \mu^{-1}\mathrm{curl}\mathbf{v}_i \cdot \left((\mathbf{A}_i - \hat{\mathbf{A}}) \times \mathbf{n}_i\right) d\mathbf{s} = 0 \tag{22}$$

to symmetrise and:

$$\sum_i \int_{\Gamma} \alpha \frac{p^2}{\mu h} \left((\mathbf{A}_i - \hat{\mathbf{A}}) \times \mathbf{n}_i\right) \cdot \left((\mathbf{v}_i - \hat{\mathbf{v}}) \times \mathbf{n}_i\right) d\mathbf{s} = 0 \tag{23}$$

to stabilise the formulation, which are zero because of equation (12), leads to:

Find $\mathbf{A}_i \in H_0(\mathrm{curl}, \Omega_i), i \in \{1, \ldots, n\}, \hat{\mathbf{A}} \in X(\Gamma)$ so that:

$$
\begin{aligned}
&\sum_i \int_{\Omega_i} \mu^{-1}\mathrm{curl}\mathbf{A}_i \cdot \mathrm{curl}\mathbf{v}_i - \kappa^2 \mathbf{A}_i \cdot \mathbf{v}_i \, d\mathbf{x} \\
&+\int_\Gamma \mu^{-1}\mathrm{curl}\mathbf{A}_i \cdot ((\mathbf{v}_i - \hat{\mathbf{v}}) \times \mathbf{n}_i) \, d\mathbf{s} \\
&+\int_\Gamma \mu^{-1}\mathrm{curl}\mathbf{v}_i \cdot \left((\mathbf{A}_i - \hat{\mathbf{A}}) \times \mathbf{n}_i\right) d\mathbf{s} \\
&+\int_\Gamma \alpha \frac{p^2}{\mu h} \left((\mathbf{A}_i - \hat{\mathbf{A}}) \times \mathbf{n}_i\right) \cdot ((\mathbf{v}_i - \hat{\mathbf{v}}) \times \mathbf{n}_i) \, d\mathbf{s} \\
&-\frac{j\omega}{Z} \int_{\Gamma_e \cup \Gamma_t} \mathbf{A}_0 \times \mathbf{n}_0 \cdot \mathbf{v}_0 \times \mathbf{n}_0 \, d\mathbf{s} \\
&= \int_{\Gamma_e} \mathbf{h} \times \mathbf{n}_0 \cdot \mathbf{v}_0 \times \mathbf{n}_0 \, d\mathbf{s}.
\end{aligned}
\tag{24}
$$

for all $\mathbf{v}_i \in H_0(\mathrm{curl}, \Omega_i), i \in \{1, \ldots, n\}, \hat{\mathbf{v}} \in X(\Gamma)$. The scalar $\alpha > 0$ represents a sufficiently large stabilisation factor of the weak formulation which is independent of the polynomial degree p of the finite element space and the mesh size h.

In simulations with a geometry where one dimension is considered as infinitely long the original vector valued problem is reduced to the scalar Helmholtz problem defined on a 2D geometry. The steps for deriving the weak formulation for the Helmholtz equation are similar to the steps for the vector potential wave equation. The biggest difference is that instead of the vector valued space $X(\Gamma)$ the scalar valued space $L^2(\Gamma)$ is needed to reinforce the field trace continuity over Γ.

3.2 Interface finite element spaces

Finite elements for the space $H_0(\mathrm{curl}, \Omega_i)$ as well as for the interface spaces $L^2(\Gamma)$ and $X(\Gamma)$ are needed. The first space is a FEM space described in (Schöberl and Zaglmayr, 2005; Zaglmayr, 2006). For the space $L^2(\Gamma)$ defined on lines in 2D, Legendre polynomials of a fixed degree are used. To discretise $X(\Gamma)$ on rectangles in 3D, tensor products of Legendre polynomials are considered. The polynomial degree for $L^2(\Gamma)$ and $X(\Gamma)$ can be chosen independently of the polynomial degree of $H_0(\mathrm{curl}, \Omega_i)$.

4. System matrix for NMFEM

The system of linear equations for the NMFEM:

$$
Mx = f \tag{25}
$$

has the following block structure:

$$
M := \begin{pmatrix}
M_{00} & M_{0\Gamma} & 0 & 0 & \cdots & 0 \\
M_{\Gamma 0} & M_{\Gamma\Gamma} & M_{\Gamma 1} & M_{\Gamma 2} & \cdots & M_{\Gamma n} \\
0 & M_{1\Gamma} & M_{11} & 0 & \cdots & 0 \\
0 & M_{2\Gamma} & 0 & M_{22} & \ddots & \vdots \\
\vdots & \vdots & \vdots & \ddots & \ddots & 0 \\
0 & M_{n\Gamma} & 0 & \ldots & 0 & M_{nn}
\end{pmatrix},
\tag{26}
$$

$$x := (x_0, x_\Gamma, x_1, x_2, \ldots, x_n)^\top, \tag{27}$$

$$f := (f_0, f_\Gamma, f_1, f_2, \ldots, f_n)^\top. \tag{28}$$

The right hand side vector can be split into f_0 corresponding to the excitation on Ω_0, f_Γ to Γ and f_i to the sub-domain Ω_i. In a similar way the unknowns x are split. Sub-blocks with mixed indices in equation (26) indicate the coupling matrices between different FE spaces. For example, the matrix $M_{0\Gamma}$ represents the coupling between the FE spaces defined on Ω_0 and Γ. Due to the identical discretisation of Ω_i, the matrices M_{ii} are identical for $i \in \{1, \ldots, n\}$. As can be seen in equation (24) the weak formulation is symmetric; therefore, the system matrix is also symmetric and $M_{i\Gamma} = M_{\Gamma i}$. These properties, as well as the structure of the system matrix, will be exploited so that the whole system matrix does not need to be assembled.

5. Schur complement

To efficiently use the introduced technique, a SC is applied to solve the resulting system of linear equations. In the SC, the inverse of the system matrix of a single sub-domain can be used for all sub-domains, reducing the computational costs. Due to the small size of the system matrix of a single sub-domain, the inverse can be cheaply calculated. The sparsity of the system matrix is retained, because the FEs on Ω_i only couple with a few degrees of freedom (DoF) on Γ.

The SC of a matrix M is defined as:

$$M = \begin{pmatrix} A & B \\ C & D \end{pmatrix} = \begin{pmatrix} I & BD^{-1} \\ 0 & I \end{pmatrix} \begin{pmatrix} A - BD^{-1}C & 0 \\ 0 & D \end{pmatrix} \begin{pmatrix} I & 0 \\ D^{-1}C & I \end{pmatrix} \tag{29}$$

and therefore the inverse of M can be written as:

$$M^{-1} = \begin{pmatrix} I & 0 \\ -D^{-1}C & I \end{pmatrix} \begin{pmatrix} (A - BD^{-1}C)^{-1} & 0 \\ 0 & D^{-1} \end{pmatrix} \begin{pmatrix} I & -BD^{-1} \\ 0 & I \end{pmatrix}, \tag{30}$$

if D is invertible. The matrix $A - BD^{-1}C$ is always invertible if the matrices M and D are invertible. For M in equation (26) the blocks are:

$$A = \begin{pmatrix} M_{00} & M_{0\Gamma} \\ M_{\Gamma 0} & M_{\Gamma\Gamma} \end{pmatrix}, \tag{31}$$

$$B = \begin{pmatrix} 0 & 0 & \cdots & 0 \\ M_{\Gamma 1} & M_{\Gamma 2} & \cdots & M_{\Gamma n} \end{pmatrix}, \tag{32}$$

$$C = \begin{pmatrix} 0 & M_{1\Gamma} \\ 0 & M_{2\Gamma} \\ \vdots & \vdots \\ 0 & M_{n\Gamma} \end{pmatrix}, \tag{33}$$

$$D = \begin{pmatrix} M_{11} & 0 & \cdots & 0 \\ 0 & M_{22} & \ddots & \vdots \\ \vdots & \ddots & \ddots & 0 \\ 0 & \cdots & 0 & M_{nn} \end{pmatrix}. \tag{34}$$

Using this approach the system of linear equations can be solved in the three steps given below for the case of two sub-domains.

5.1 Pre-processing
The first step has the form:

$$\begin{pmatrix} I & -BD^{-1} \\ 0 & I \end{pmatrix} f = \begin{pmatrix} I & 0 & 0 & 0 \\ 0 & I & -M_{\Gamma 1}(M_{11})^{-1} & -M_{\Gamma 2}(M_{22})^{-1} \\ 0 & 0 & I & 0 \\ 0 & 0 & 0 & I \end{pmatrix} \begin{pmatrix} f_0 \\ f_\Gamma \\ f_1 \\ f_2 \end{pmatrix} = \begin{pmatrix} f_0 & \tilde{f}_\Gamma & f_1 & f_2 \end{pmatrix}^\top =: \tilde{f}. \tag{35}$$

As can be seen, only f_Γ is altered. To assemble the necessary matrices $M_{\Gamma i}(M_{ii})^{-1}$ systems of linear equations with M_{ii} have to be solved. The total number of needed solutions is equal to the number of degrees of freedom (N_{DOF}) of the boundary space on $\Gamma \cap \partial\Omega_i$. This might be time expensive depending on the size of the sub-domain discretisation matrix and on the N_{DOF} on the boundary, but due to the identical discretisation of each Ω_i and of the boundary spaces around the sub-domains, the matrices $M_{\Gamma i}(M_{ii})^{-1}$ are, up to permutations, identical for all sub-domains and therefore only one needs to be assembled.

5.2 Solving
The second step is given by:

$$\begin{pmatrix} (A - BD^{-1}C)^{-1} & 0 \\ 0 & D^{-1} \end{pmatrix} \tilde{f} = \begin{pmatrix} S^{-1} & 0 & 0 \\ 0 & (M_{11})^{-1} & 0 \\ 0 & 0 & (M_{22})^{-1} \end{pmatrix} \begin{pmatrix} f_0 \\ \tilde{f}_\Gamma \\ f_1 \\ f_2 \end{pmatrix} = \begin{pmatrix} x_0 \\ x_\Gamma \\ \tilde{x}_1 \\ \tilde{x}_2 \end{pmatrix} =: \tilde{x}, \tag{36}$$

Where:

$$S := \begin{pmatrix} M_{00} & M_{0\Gamma} \\ M_{\Gamma 0} & M_{\Gamma\Gamma} - \sum_{i=1}^{2} M_{\Gamma i}(M_{ii})^{-1} M_{i\Gamma} \end{pmatrix}. \tag{37}$$

Instead of one large system of linear equations, smaller systems of linear equations on the individual sub-domains can be considered in parallel. On the sub-domains solutions with M_{ii} have to be calculated. On the exterior domain a system of linear equations with S has to be solved. To assemble the matrices $M_{\Gamma i}(M_{ii})^{-1}M_{i\Gamma}$ in S the matrix $M_{\Gamma i}(M_{ii})^{-1}$, which has already been assembled in the first step, can be used.

5.3 Post-processing

The third step consists of:

$$\begin{pmatrix} I & 0 \\ -D^{-1}C & I \end{pmatrix} \hat{x} = \begin{pmatrix} I & 0 & 0 & 0 \\ 0 & I & 0 & 0 \\ 0 & -(M_{11})^{-1}M_{1\Gamma} & I & 0 \\ 0 & -(M_{22})^{-1}M_{2\Gamma} & 0 & I \end{pmatrix} \begin{pmatrix} x_0 \\ x_\Gamma \\ \tilde{x}_1 \\ \tilde{x}_2 \end{pmatrix} = \begin{pmatrix} x_0 \\ x_\Gamma \\ x_1 \\ x_2 \end{pmatrix}. \tag{38}$$

In this step only the solution vectors of the sub-domains are altered. Due to the symmetry of the system matrix, the matrix assembled in the first step can be used for the third step.

In case of no excitations on the sub-domains, $f_i = 0, i \in \{1, \ldots, n\}$, the first step can be omitted. If the solution on the sub-domains is not needed, the third step can be neglected.

6. Numerical example

To show the feasibility of the introduced method, 2D and 3D ventilation grills have been considered.

6.1 2D Ventilation grill with one aperture

As a 2D example, a ventilation grill with one aperture, see Figure 4, has been chosen. The shielding Γ_D has been modelled by homogeneous Dirichlet boundary conditions. Homogeneous Neumann boundary conditions have been applied on Γ_N. The bottom boundary Γ_t has been considered as transparent and modelled by first order absorbing boundary conditions (ABC) (Chatterjee *et al.*, 1993). On the boundary Γ_e at the top a plane wave and a first order ABC have been applied via a Robin boundary condition with $\mathbf{h} = \left(\frac{j\omega}{Z}, 0\right)^\top$. The permeability and permittivity of vacuum have been used and a frequency $f = 10\,GHz$ is considered. The reference solution with FEM and the solution with NMFEM have been compared. The logarithmically scaled norm of the solutions can be seen in Figure 4. The relative L^2 error on Ω_0 of the NMFEM solution is:

$$\frac{||A_{ref} - A_{NMFEM}||_{L^2(\Omega_0)}}{||A_{ref}||_{L^2(\Omega_0)}} \cdot 100\% = 0.06\%. \tag{39}$$

6.2 3 D Ventilation grill with 25 apertures

As a more realistic 3 D example, a ventilation grill with 5×5 apertures, see Figure 5 and 6, has been considered.

The boundary value problem equation (24) has been solved at the frequency $f = 10\,GHz$. For the permeability μ and the permittivity ε vacuum has been chosen. The excitation has been set to:

$$\mathbf{h} = \left(\exp\left(-\frac{(x-20)^2}{100^2} \right), 0, 0 \right)^\top . \tag{40}$$

Although, for instance, perfectly matched layers (Leumüller *et al.*, 2019) would be more accurate, for the sake of simplicity first-order absorbing conditions have been prescribed on the outer boundary $\Gamma_t \cup \Gamma_e$. The shielding Γ_D has been modelled by homogeneous Dirichlet boundary conditions. Finally, this work focuses on upscaling and DD. The solution with the NMFEM on the exterior domain can be seen in Figure 7. All the numerical examples have been calculated with the aid of the open source FE software Netgen/NGSolve (Schöberl, 2022).

The computational times for the FEM simulation and the NMFEM simulation have been compared. A constant maximum size for the mesh elements has been chosen in all simulations. The meshes around the apertures are still very fine in the simulations. For the $H(\mathrm{curl})$ FE spaces the polynomial degree has been set to $p = 3$ in all simulations. The polynomial degree of the boundary FE space on Γ has been set to $p_\Gamma = 6$. All calculations have been carried out on 16 cores in parallel. As a solver for the systems of linear equations, PARDISO (De Coninck *et al.*, 2016; Verbosio *et al.*, 2017; Kourounis *et al.*, 2018) has been used. The number of sub-domains N_{SD} has been varied between $N_{SD} \in \{1, 4, 9, 16, 25\}$. A list of the N_{DOF} for the different simulations can be seen in Table 1. In Figure 8 the simulation times for NMFEM and FEM are shown. For small N_{SD} the computation time for the sub-domain matrices in the SC, e.g. $M_{\Gamma i}(M_{ii})^{-1}$, is dominant, but for a more realistic number of apertures the factorisation and solving with PARDISO dominate. In the FEM simulation the computation time

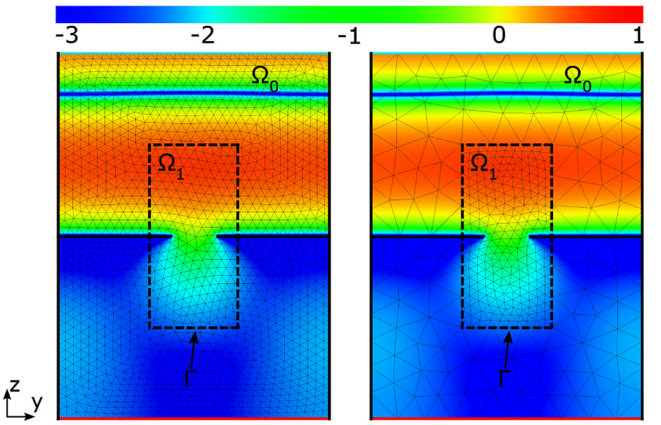

Figure 4.
Reflection and transmission of an incident plane wave from above of the aperture, reference solution with fine mesh (left), domain decomposition solution with upscaling i.e. fine and coarse mesh (right)

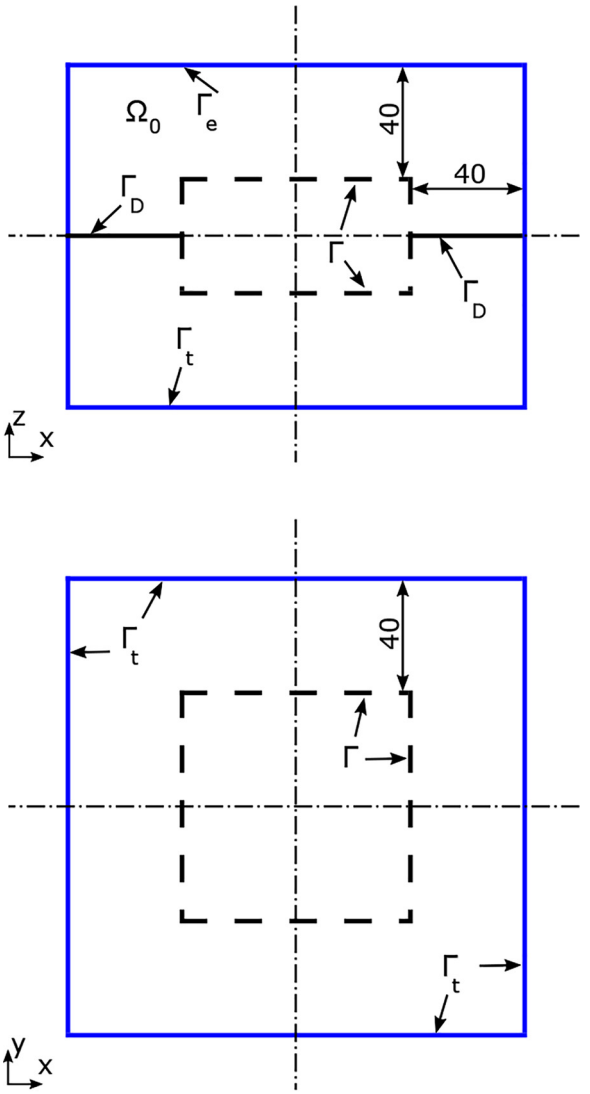

Note: The region comprising sub-domains is indicated by dashed lines, front view (above) and top view (below); all dimensions are in mm. Solid blue lines represent the outer boundary; dashdotted lines are planes of symmetry

Figure 5.
Geometry of the exterior domain of a ventilation grill

is always dominated by the factorisation and solving with PARDISO. The meshing and assembling times for the system matrices are small in comparison to the factorisation times. The maximal used memory for NMFEM and FEM with respect to N_{SD} can be seen in Figure 9. Using NMFEM the maximal memory demands are enormously reduced.

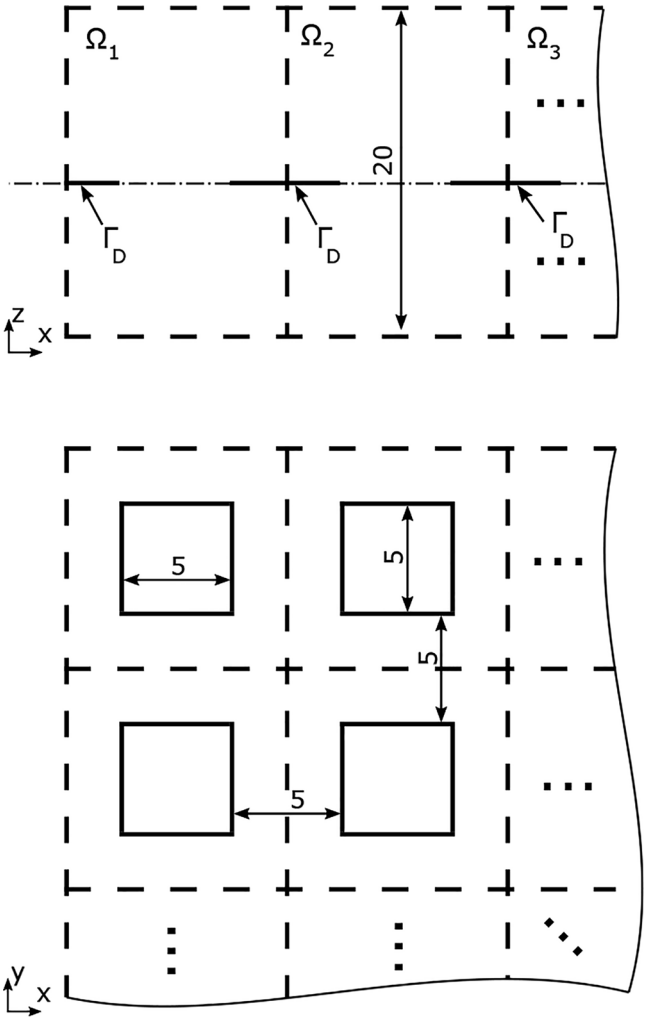

Note: Three dots represent a periodic extension to further sub-domains, all dimensions are in mm

Figure 6.
Geometry of the periodic sub-domains with quadratic openings; boundaries between the sub-domains are indicated by dashed lines, front view (above) and top view (below)

7. Conclusion

A NMFEM with non-matching meshes for 2D and 3D ventilation grills with quasi-periodic apertures has been introduced. The method leads to a large reduction of the computational time and the memory demands through upscaling and SC reduction. This has been achieved by an efficient implementation of the SC. The identical discretisation of each sub-domain has been essential to decrease the N_{DOF} in the simulations.

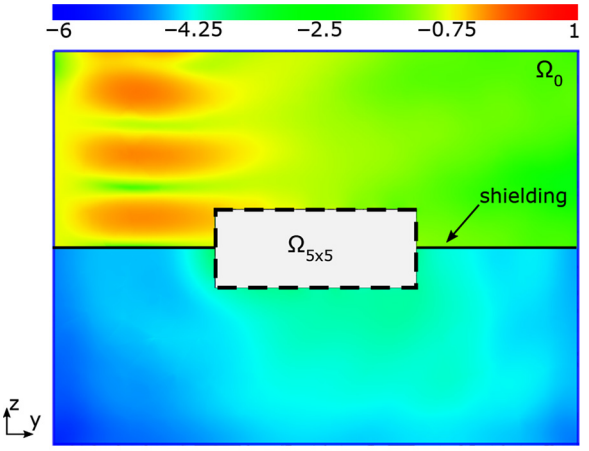

Note: The logarithmically scaled norm of the magnetic vector potential is shown

Figure 7. Incident, reflected and transmitted field of a plane wave impinging a shielding with an array of 5 × 5 apertures

N_{SD}	1	4	9	16	25
NMFEM					
N_{DOF,Ω_e}	21,908	40,384	80,348	126,092	164,432
$N_{DOF,\Gamma}$	432	1,440	3,024	5,184	7,920
N_{DOF,Ω_i}	19,060	19,060	19,060	19,060	19,060
$N_{DOF,\Gamma\cap\partial\Omega_i}$	432	432	432	432	432
FEM N_{DOF}	66,000	187,824	408,048	707,364	1,073,208

Table 1. The NDOF for NMFEM and FEM with respect to the number of subdomains

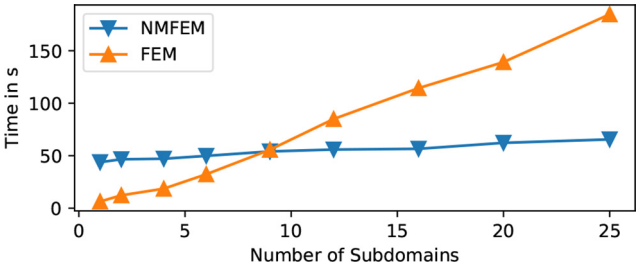

Figure 8. Computation time for solving with the NMFEM and the FEM with respect to the number of subdomains

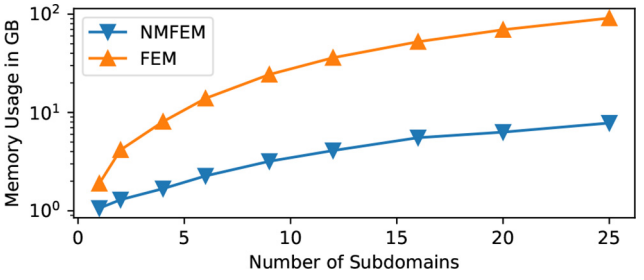

Figure 9. Maximal memory requirement in gigabyte (GB) for solving with the NMFEM and the FEM with respect to the number of subdomains

References

Ali, S., Weile, D. and Clupper, T. (2005), "Effect of near field radiators on the radiation leakage through perforated shields", *IEEE Transactions on Electromagnetic Compatibility*, Vol. 47 No. 2, pp. 367-373.

Araneo, R. and Lovat, G. (2009), "Fast MoM analysis of the shielding effectiveness of rectangular enclosures with apertures, metal plates and conducting objects", *IEEE Transactions on Electromagnetic Compatibility*, Vol. 51 No. 2, pp. 274-283.

Bardi, I., Vogel, M. and Cendes, Z.J. (2006), "Modeling large screens via homogenization with the finite element method", *2006 IEEE MTT-S International Microwave Symposium Digest*, pp. 1315-1318.

Boubekeur, M., Kameni, A., Bernard, L., Modave, A. and Pichon, L. (2014), "3-D modeling of thin sheets in the discontinuous Galerkin method for transient scattering analysis", *IEEE Transactions on Magnetics*, Vol. 50 No. 2, pp. 493-496.

Carpes, W., Ferreira, G., Raizer, A., Pichon, L. and Razek, A. (2000), "TLM and FEM methods applied in the analysis of electromagnetic coupling", *IEEE Transactions on Magnetics*, Vol. 36 No. 4, pp. 982-985.

Chatterjee, A., Jin, J.M. and Volakis, J.L. (1993), "Edge-based finite elements and vector ABCs applied to 3-D scattering", *IEEE Transactions on Antennas and Propagation*, Vol. 41 No. 2, pp. 221-226.

Cockburn, B., Gopalakrishnan, J. and Lazarov, R. (2009), "Unified hybridization of discontinuous Galerkin, mixed and continuous Galerkin methods for second order elliptic problems", *SIAM Journal on Numerical Analysis*, Vol. 47 No. 2, pp. 1319-1365.

Cruciani, S., Feliziani, M. and Maradei, F. (2015), "Prediction of shielding effectiveness in graphene enclosures by FEM-INBC method", *2015 Asia-Pacific Symposium on Electromagnetic Compatibility (APEMC)*, pp. 376-379.

De Coninck, A., De Baets, B., Kourounis, D., Verbosio, F., Schenk, O., Maenhout, S. and Fostier, J. (2016), "Needles: toward large-scale genomic prediction with marker-by-environment interaction", *Genetics*, Vol. 203 No. 1, pp. 543-555, doi: 10.1534/genetics.115.179887.

Georgakopoulos, S., Birtcher, C. and Balanis, C. (2001), "HIRF penetration through apertures: FDTD versus measurements", *IEEE Transactions on Electromagnetic Compatibility*, Vol. 43 No. 3, pp. 282-294.

Graham, I. and Scheichl, R. (2007), "Robust domain decomposition algorithms for multi scale PDEs", *Numerical Methods for Partial Differential Equations*, Vol. 23 No. 4, pp. 859-878, doi: 10.1002/num.20254.

Heinrich, B. and Nicaise, S. (2001), "The Nitsche mortar finite-element method for transmission problems with singularities", *IMA Journal of Numerical Analysis*, Vol. 23 No. 2, pp. 331-358.

Hollaus, K., Feldengut, D., Schöberl, J., Wabro, M. and Omeragic, D. (2010), "Nitsche-type mortaring for Maxwell's equations", *PIERS 2010 Cambridge – Progress in Electromagnetics Research Symposium, Proceedings*.

Holloway, C.L. and Kuester, E.F. (2018), "Generalized sheet transition conditions for a meta screen – a fishnet meta surface", *IEEE Transactions on Antennas and Propagation*, Vol. 66 No. 5, pp. 2414-2427.

Jiao, C., Li, L., Cui, X. and Li, H. (2006), "Subcell FDTD analysis of shielding effectiveness of a thin-walled enclosure with an aperture", *IEEE Transactions on Magnetics*, Vol. 42 No. 4, pp. 1075-1078.

Kourounis, D., Fuchs, A. and Schenk, O. (2018), "Towards the next generation of multi period optimal power flow solvers", *IEEE Transactions on Power Systems*, Vol. 33 No. 4, pp. 4005-4014, doi: 10.1109/TPWRS.2017.2789187.

Kubík, Z. and Skála, J. (2015), "Shielding effectiveness measurement and simulation of small perforated shielding enclosure using FEM", *2015 IEEE 15th International Conference on Environment and Electrical Engineering (EEEIC)*, pp. 1983-1988.

Leumüller, M., Auinger, B., Hackl, H., Schöberl, J. and Hollaus, K. (2019), "Imperfect EM shielding by thin conducting sheets with PEC and SIBC", *2019 22nd International Conference on the Computation of Electromagnetic Fields (COMPUMAG)*, pp. 1-4.

Li, M., Nuebel, J., Drewniak, J., DuBroff, R., Hubing, T. and Van Doren, T. (2000), "EMI from airflow aperture arrays in shielding enclosures-experiments, FDTD and MoM modeling", *IEEE Transactions on Electromagnetic Compatibility*, Vol. 42 No. 3, pp. 265-275.

Nie, B.L., Du, P.A., Yu, Y.T. and Shi, Z. (2011), "Study of the shielding properties of enclosures with apertures at higher frequencies using the transmission-line modeling method", *IEEE Transactions on Electromagnetic Compatibility*, Vol. 53 No. 1, pp. 73-81.

Schöberl, J. (2022), "NetGen/NGSolve", available at: https://ngsolve.org

Schöberl, J. and Zaglmayr, S. (2005), "High order Nédélec elements with local complete sequence properties", *Compel – the International Journal for Computation and Mathematics in Electrical and Electronic Engineering*, Vol. 24 No. 2, pp. 374-384.

Verbosio, F., Coninck, A.D., Kourounis, D. and Schenk, O. (2017), "Enhancing the scalability of selected inversion factorization algorithms in genomic prediction", *Journal of Computational Science*, Vol. 22, pp. 99-108, doi: 10.1016/j.jocs.2017.08.013.

Zaglmayr, S. (2006), "High order finite element methods for electromagnetic field computation", Ph.D. dissertation, Johannes Kepler University Linz.

Corresponding author
Michael Leumüller can be contacted at: michael.leumueller@tuwien.ac.at